CARLETON UNIVERSITY

SCHOOL OF
MATHEMATICS AND STATISTICS

HONOURS PROJECT

TITLE: Modelling Population Dynamics of Neurons and Epilepsy

AUTHOR: Katherine Cho

SUPERVISOR: David Amundsen

DATE: August 6th, 2021

1 Introduction

1.1 Modelling Neurons

A model can be described as a practical analogy of a real life problem. For example in your brain there are cells called neurons. Each individual neuron can be modelled by a battery. Neurons receive, integrate and transmit information in the human brain. Like a battery, neurons have electrochemical reactions called neural impulses. The positive and negative ions move at different rates.

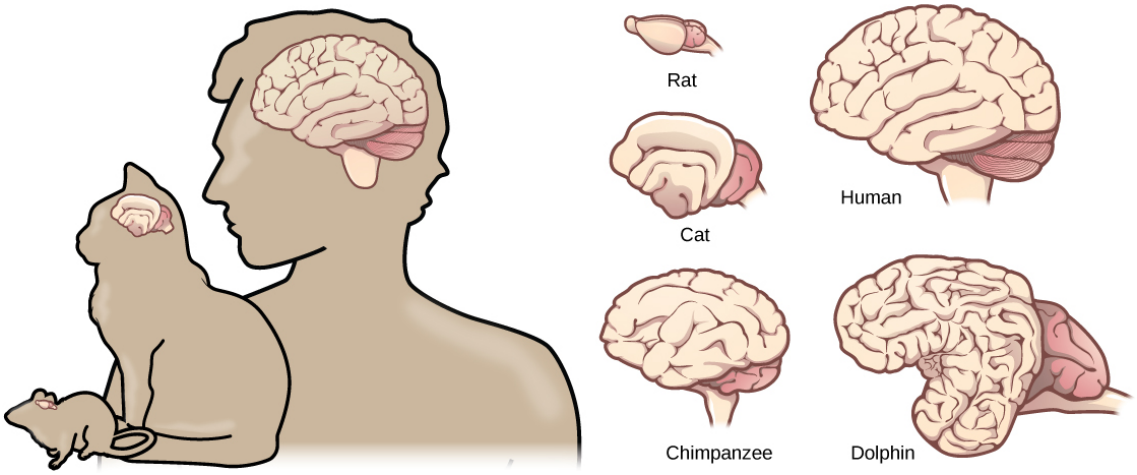

Figure 1: Human vs animal brain ([1] fig 16.23)

The human brain is incredibly complex with billions of interacting cells. As seen in Figure 1, due to the differences between the human brain and various animal brains, the focus will be on human brains.These cells coordinate how your body moves, integrates information and enables speech, planning, remembering, dreaming, creating and thinking. The brain consists of the hindbrain, midbrain and forebrain. The cerebrum is the section of the forebrain that deals with activities such as thinking, learning and planning [2]. The cerebral cortex is the outer layer of the cerebrum. This is where the excitatory and inhibitory neurons are located.

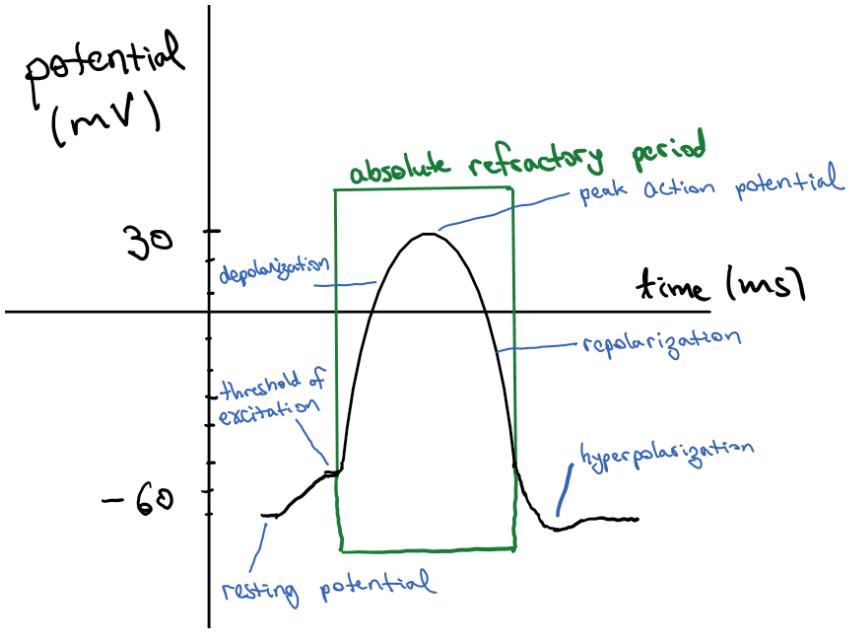

Figure 2: Action potential of a neuron can be divided into 5 steps: (i.) Resting potential. (ii.) Threshold of excitation. (iii.) Peak action potential. (iv.) Hyperpolarization. (v.) Return to resting potential.

When a neuron is at rest and not sending a message, the voltage is constant. An action potential is a change in electric charge of a neuron. As seen in Figure 2, an action potential has several steps. The neuron receives a stimulus, and then the threshold of excitation is reached. The potential becomes less negative, this is called depolarization. This occurs until the peak action potential is reached. The time taken for depolarization and repolarization is known as the absolute refractory period, lasting 1-2 milliseconds.The absolute refractory period is the gree box in Figure 2. Then repolarization occurs, where the cell attempts to return to the original voltage. As this occurs, the cell hyperpolarizes, where the potential becomes lower than resting state temporarily. This time is known as the relative refractory period. An action potential is an all or nothing process, either the neuron fires or it does not. This firing can send a message, excitatory or inhibitory. Since excitatory neurons have a positive voltage, this leads to a greater chance of firing. On the other hand, inhibitory neurons have a negative voltage, leading to a lower chance of firing [2].

1.2 Epilepsy

Epilepsy is a neurological disorder with recurrent seizures. It can be diagnosed using an electroencephalograph (EEG), a procedure where electrodes on the scalp record the brain's elec-

trical activity [2]. The abnormal brain activity seen on the recording indicates the occurrence of a seizure. Currently mechanisms behind seizures is not known [3]. Epilepsy is treated with antiepileptic drugs [4] with surgery being a last resort. An important historical case is patient H. M. who had parts of his brain removed due to epilepsy. While the surgery did help with the seizures, it left him with anterograde amnesia(the inability to form new long-term memories) [5].

1.3 Mathematical Modelling

Mathematical models seek to represent problems using equations. The complexity can vary from a few equations to hundreds [6]. A model with only a handful of equations might be more general and/or less accurate compared to a model with more equations. This report looks at two papers [3] and [7] discussing the modelling of epilepsy using the Wilson-Cowan model. The model was developed in 1972 by Hugh Wilson and Jack Cowan. A system of differential equations is used to model interactions between a local population of excitatory and inhibitory neurons [5]. Some assumptions are made so that mathematical models can be generalized and are not overly complex [6].

1.4 Mean Field Theory

Coarse-graining is a technique that considers a model(system) at a lower resolution. This is done by seeking to represent the model by excluding information that is not crucial [8]. An example is gas molecules in a closed room. Ensuring the comfort of the room is possible using coarse-graining measures of pressure, temperature and density of the relative molecules. The dynamics of all of the molecules are not relevant [8].

Mean field theory is a coarse-graining approach that was initially used for magnetism. This involves the movement and alignment of atomic spins. To simplify matter, if the number of spins is sufficiently high and uncorrelated, then by the central limit theorem (Theorem 1) the fluctuations go down to zero. Mean then becomes the relevant quantity, hence the name. Similarly to atoms, interactions between neurons are negligible.

Theorem 1 *(Central limit theorem) Let $X_1, X_2, ..., X_n$ be independent and identically distributed random variables with mean, $E[X_i] = \mu$ and variance, $V[X_i] = \sigma^2 < \infty$ for $i = 1, 2, ..., n$ where $Z_n = \frac{\bar{X}-\mu}{\sigma/\sqrt{n}} = \frac{\sum_{i=1}^{n} X_i - n\mu}{\sqrt{n}\sigma}$ Then the distribution function of Z_n converges to the standard normal distribution function as n goes to ∞.*

Temporal coarse-graining is a technique used for simplification in statistical physics [5]. The main idea is to replace some dependent variable $f(t)$ by moving the time average over some interval s. Then,

$$\bar{f}(t) = \frac{1}{s}\int_{t-s}^{t} f(t')dt' \tag{1}$$

is the coarse-grained variable.

1.5 Phase Portraits

Let

$$\frac{dx}{dt} = f(x,y) \tag{2}$$

$$\frac{dy}{dt} = g(x,y) \tag{3}$$

be a system of nonlinear equations.

Nullclines are curves in the xy plane. While not solution curves, they do provide insight on solution trajectories [6]. A curve in the phase plane in which $\frac{dx}{dt} = 0$ is called a x-nullcline. Here $x(t)$ is fixed while $y(t)$ changes. Respectively a y-nullcline is a curve in the plane on which $\frac{dy}{dt} = 0$. The region where $f(x,y) < 0$ is where $\frac{dx}{dt} < 0$ and $x(t)$ is decreasing in the direction of the arrow ($\leftarrow$). When $f(x,y) > 0$, $x(t)$ is increasing in the ($\rightarrow$) direction. The region where $g(x,y) < 0$ and $\frac{dy}{dt} < 0$, is where $y(t)$ is decreasing downwards while $g(x,y) > 0$ is where $y(t)$ is increasing in the upwards direction. The point where the nullclines intersect are the equilibrium points.

The equilibrium points (x_*, y_*) are when $f(x_*, y_*) = g(x_*, y_*) = 0$. The nonlinear system can be linearized by approximating $f(x,y), g(x,y)$ when (x,y) is close to (x_*, y_*). Let

$$u = x - x_* \tag{4}$$

$$v = y - y_* \tag{5}$$

Then

$$\frac{du}{dt} = \frac{dx}{dt} = f(x,y) = f(x_* + u, y_* + v) \tag{6}$$

$$\frac{dv}{dt} = g(x_* + u, y_* + v) \tag{7}$$

Then using Taylor expansions of f and g,

$$f(x_* + u, y_* + v) = f(x_*, y_*) + f_x(x_*, y_*)u + f_y(x_*, y_*)v + ... \tag{8}$$

$$g(x_* + u, y_* + v) = g(x_*, y_*) + g_x(x_*, y_*)u + g_y(x_*, y_*)v + ... \tag{9}$$

Then assuming f and g are differentiable near (x_*, y_*) the system becomes,

$$\frac{du}{dt} = f_x(x_*, y_*)u + f_y(x_*, y_*)v \tag{10}$$

$$\frac{dv}{dt} = g_x(x_*, y_*)u + g_y(x_*, y_*)v \tag{11}$$

$$\begin{bmatrix} \frac{du}{dt} \\ \frac{dv}{dt} \end{bmatrix} = \begin{bmatrix} f_x(x_*, y_*) & f_y(x_*, y_*) \\ g_x(x_*, y_*) & g_y(x_*, y_*) \end{bmatrix} \begin{bmatrix} u \\ v \end{bmatrix} \tag{12}$$

The Jacobian matrix at equilibrium points is given by

$$J(x_*, y_*) = \begin{bmatrix} f_x(x_*, y_*) & f_y(x_*, y_*) \\ g_x(x_*, y_*) & g_y(x_*, y_*) \end{bmatrix} \tag{13}$$

The phase plane can be analysed at each point. The trace and determinant of the Jacobian matrix at each point give the type of point and whether the point is stable or not as seen in Figure 3. This is for the case of two equations and can be generalized for higher dimensions.

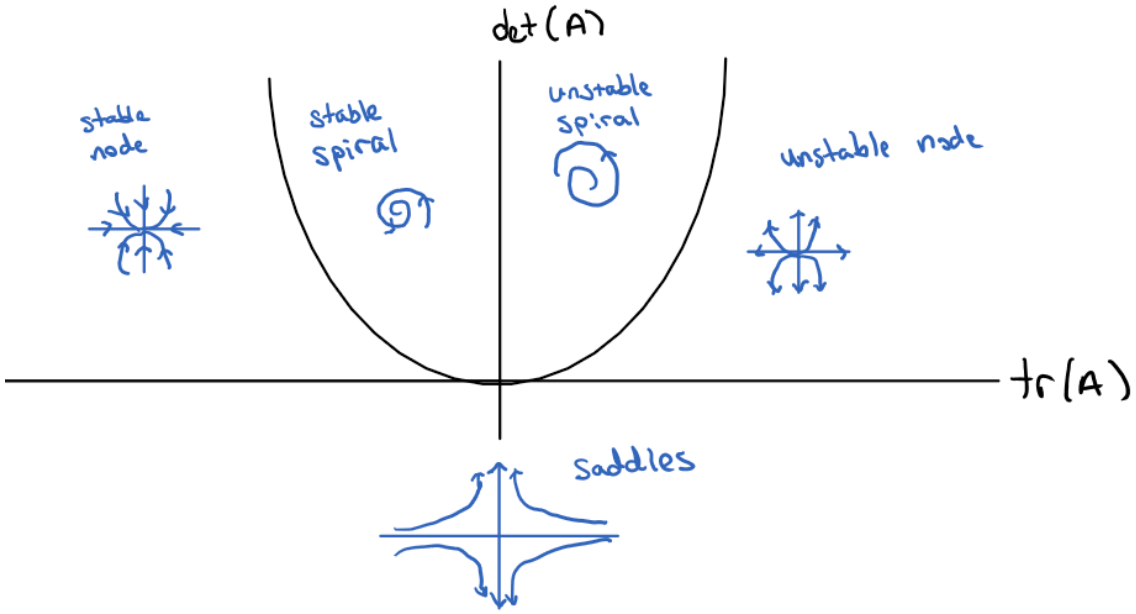

Figure 3: Summary of phase plane diagrams dependent on trace and determinant of some matrix A.

1.6 Introduction to Bifurcation Theory

Taking a nonlinear system of differential equations and linearizing, gives phase portraits for each equilibrium point. If a parameter's value is changed and this changes the type of equilibrium

point, then this is called a bifurcation. The value at which the parameter changes is called the bifurcation value. A bifurcation diagram is a graph with the horizontal axis representing the bifurcation values. The vertical axis is the location of the equilibrium point(s). Generally stable states are indicated by solid lines and unstable by dashed lines [9].

There are several types of bifurcations,

i. A saddle-node bifurcation is when a pair of points collide or appear to do so.

ii. A transcritical bifurcation is when one point passes through another. The points usually exchange stabilities.

iii. A pitchfork bifurcation has two forms. A supercritical pitchfork bifurcation is when one stable fixed point splits into three fixed points with the outer two being stable. A subcritical pitchfork bifurcation is one unstable that splits into 3 points, with two of them being unstable.

iv. A Hopf bifurcation is when a limit cycle appears or disappears around an equilibrium point. A limit cycle is closed curves in the phase plane. The limit cycle is stable if all other curves move towards it as time approaches positive infinity.

Figure 4 gives examples of bifurcation diagrams. Figure 4a is a saddle-node bifurcation and Figure 4b is transcritical bifurcation. A supercritical pitchfork bifurcation can be seen in Figure 4c and a subcritical one in Figure 4d. Two types of Hopf bifurcations are seen in Figure 4e and Figure 4f. The limit cycle is in blue.

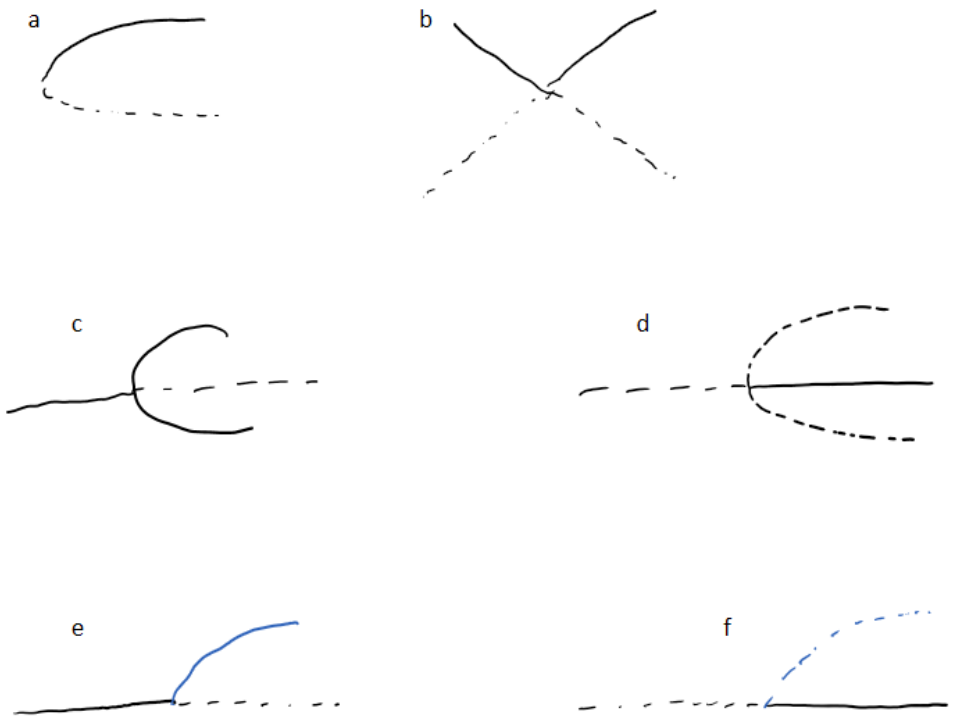

Figure 4: Bifurcation diagrams. (a) saddle-node bifurcation. (b) transcritical bifurcation. (c) supercritical pitchfork bifurcation. (d) subcritical pitchfork bifurcation. (e) and (f) Hopf bifurcation with limit cycle (blue)

2 Wilson-Cowan Model

Using physics and the motion of fluid as an analogy, the Wilson-Cowan model seeks to model the local population dynamics of neurons. When looking at fluid at the molecular level, brownian motion is seen. When observing macroscopically, the flow is streamlined. This model looks at the properties of cell populations instead of individual cells [5]. The assumptions made for this model are

i. any local population contains both excitatory and inhibitory neurons

ii. time is continuous

iii. spatial interactions are neglected

2.1 Derivation

Based on [5], let $E(t)$ be defined as the proportion of excitatory cells firing per unit time at the instance t and $I(t)$ as the proportion of inhibitory cells firing per unit time at the instance t. These proportions are dependent on the non-refractory (ie. sensitive cells) and the proportion on cells receiving threshold excitation. Low levels of background activity will be at the state $E(t), I(t) = 0$, the resting state. When E and I are small and negative values, they represent the depression of resting activity and have physiological significance.

Let r be the absolute refractory period in milliseconds. This is the minimum duration after an action potential occurs and the next one begins. For simplification the relative refractory period can be assumed to be 0 (see appendix in [5]). To derive $E(t)$ and $I(t)$, assume that the values of the functions at time $(t+r)$ are equal to the proportion of non-refractory excitatory(respectively inhibitory) cells and which also receive a minimum threshold excitation at t.

Then,

$$\int_{t-r}^{t} E(t')dt' \tag{14}$$

gives the proportion of refractory excitatory cells at time, t. Respectively the proportion of non-refractory excitatory cells is given by

$$1 - \int_{t-r}^{t} E(t')dt' \tag{15}$$

2.1.1 Subpopulation response function

The expected proportion of cells in a subpopulation that would respond if not initially in an absolute refractory state is given by $S_\epsilon(x)$and $S_i(x)$, the respective subpopulation response functions for $E(t)$ and $I(t)$.

Assuming that there is a a distribution of neural threshold excitement denoted by the distribution function $D(\theta)$, then $S(x)$ is given by

$$S(x) = \int_{0}^{x(t)} D(\theta)d\theta \tag{16}$$

where $x(t)$ is the average excitation since all cells receive the same number of impulses. Since $S(x)$ is monotonically increasing function of $x(t)$, an assumption that $S(x)$ is a sigmoid function can be made. In general a function, $f(x)$ is said to be a sigmoid function if it has the following properties

i. $f(x)$ is monotonically increasing

ii. $f(x)$ has asymptotic values at 1 and 0 as it approaches $-\infty$ and ∞

iii. $f(x)$ has one inflection point

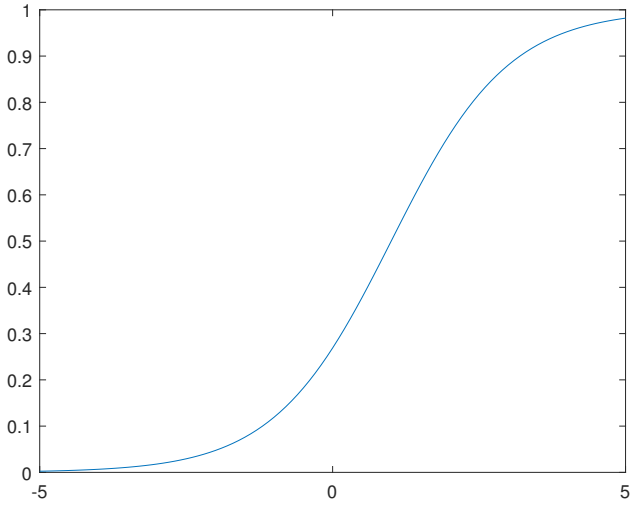

Figure 5: Sigmoid Function

The subpopulation response function is a sigmoid function and the following can be observed regarding the shape

i. If the level of excitement is too low, the threshold elements will not be excited. On the other hand, all the elements will be excited if the level is too high.

ii. Numerous studies have show that both single cell response curves and and population response curves are sigmoid functions.

Taking the sum of all the individual cell's input along with simulation decay and time course $\alpha(t)$ which is a response function representing the time evolution of neural spikes. Then the average level of excitation at time, t for excitatory cells is given by

$$\int_{-\infty}^{t} \alpha(t-t')[c_1 E(t') - c_2 I(t') + P(t')]dt' \tag{17}$$

where $c_1, c_2 > 0$ are the connectivity coefficients representing the average number of excitatory and inhibitory synapses per cell and $P(t)$ is the external input. For inhibitory cells it is

$$\int_{-\infty}^{t} \alpha(t-t')[c_3 E(t') - c_4 I(t') + Q(t')]dt' \tag{18}$$

where $c_3, c_4 > 0$ are the connectivity coefficients representing the average number of excitatory and inhibitory synapses per cell and $Q(t)$ is the external input. The external input will be varied throughout the analysis with values ranging from -1 to 2.

The probability of a cell being sensitive is independent of the probability of a cell being excited and a correlation equation is added. However in this case the correlation is taken to be 0 and, the equations for population dynamics of a local population are given by

$$E(t+\tau) = \left[1 - \int_{t-r}^{t} E(t')dt'\right] S_\epsilon \left[\int_{-\infty}^{t} \alpha(t-t')[c_1 E(t') - c_2 I(t') + P(t')]dt'\right] \tag{19}$$

$$I(t+\tau') = \left[1 - \int_{t-r}^{t} I(t')dt'\right] S_i \left[\int_{-\infty}^{t} \alpha(t-t')[c_3 E(t') - c_4 I(t') + Q(t')]dt'\right] \tag{20}$$

where τ and τ' are response delays.

2.1.2 Time coarse-graining

The above equations are complex and can be simplified using a technique called temporal coarse-graining as seen in equation (1).

$$\int_{t-r}^{r} E(t')dt' \to r\bar{E}(t) \tag{21}$$

$$\int_{-\infty}^{t} \alpha(t-t')E(t')dt' \to k\bar{E}(t) \tag{22}$$

where r and k are constants with $k = \int_{-\infty}^{t} \alpha(t-t')dt'$.

Taking Taylor expansions of $E(t+\tau)$ and $I(t+\tau')$ around $\tau = 0$ gives

$$\tau\frac{d\bar{E}}{dt} = -\bar{E} + [1 - r\bar{E}]S_\epsilon[kc_1\bar{E} - c_2 k\bar{I} + kP(t)] \tag{23}$$

$$\tau\frac{d\bar{I}}{dt} = -\bar{I} + [1 - r\bar{I}]S_i[k'c_3\bar{E} - c_4 k\bar{I} + k'Q(t)] \tag{24}$$

Adding back the interaction with the inhibitory population gives

$$\tau\frac{dE}{dt} = -E[1 - \int_{t-r}^{t} E(t')dt']S_\epsilon \left[\int_{-\infty}^{t} e^{t-t'}[c_1 E(t') + P(t')]dt'\right] \tag{25}$$

$$\tau\frac{d\bar{E}}{dt} = -\bar{E}[1 - r\bar{E}]S_\epsilon[kc_1\bar{E} + kP(t)] \tag{26}$$

2.2 Analysis

Noting that if $P(t), Q(t) = 0$, then $\bar{E} = \bar{I} = 0$ is a steady state. Further simplification occurs by setting $S_\epsilon(0) = 0$ and $I_i(0) = 0$ by subtracting $S(0)$ from the subpopulation response functions.

Dropping the bars for convenience gives,

$$\tau_\epsilon \frac{dE}{dt} = -E + (k_\epsilon - r_\epsilon E) S_\epsilon (c_1 E - c_2 I + P) \tag{27}$$

$$\tau_i \frac{dI}{dt} = -I + (k_i - r_i I) S_i (c_3 E - c_4 I + Q) \tag{28}$$

where k_ϵ and k_i are the result of the modified refractory terms. Taking S_ϵ^{-1} and S_i^{-1} as the unique inverses of the sigmoid functions then,

$$c_2 I = c_1 - S_\epsilon^{-1} \left[\frac{E}{k_\epsilon - r_\epsilon E} \right] + P \tag{29}$$

$$c_3 E = c_4 I + S_i^{-1} \left[\frac{I}{k_i - r_i I} \right] - Q \tag{30}$$

are the equations for the nullclines when $dE/dt = 0$ and $dI/dt = 0$. This can be seen in figure 6 where $c_1 = 12$, $c_2 = 4$, $c_3 = 13$, $c_4 = 11$, $a_\epsilon = 1.2$, $\theta_\epsilon = 2.8$, $a_i = 1$, $\theta_i = 4$, $r_\epsilon = r_i = 1$ and $P = Q = 0$. Here the (+) denotes stable states.

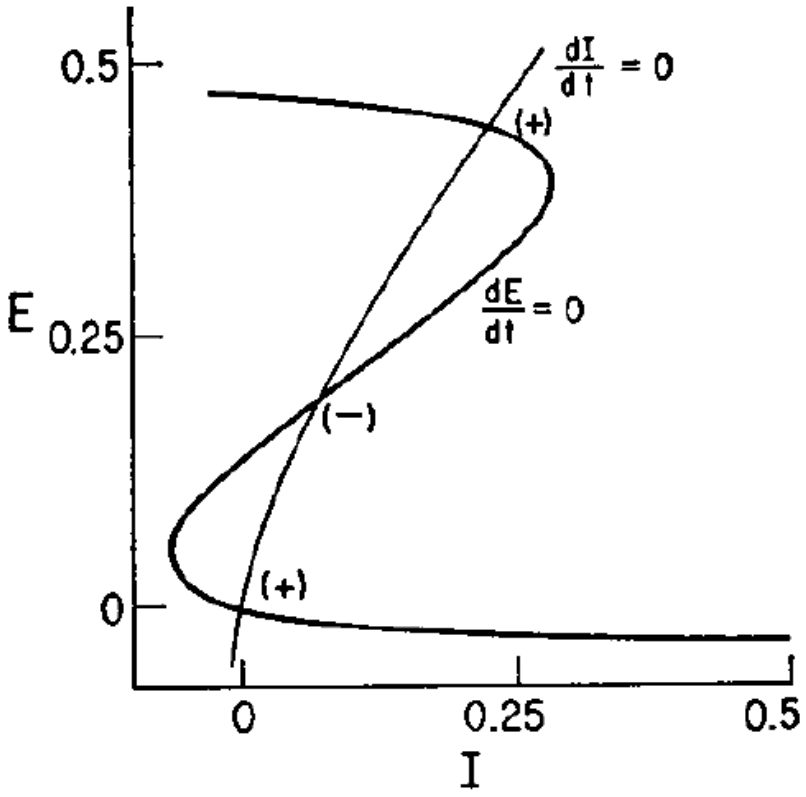

Figure 6: Nullclines for equations (29) and (30). The stable states are denoted by (+) and unstable ones by (-). ([5] fig 4)

Taking the subpopulation response function as

$$S(x) = \frac{1}{1 + exp(-a(x - \theta))} \tag{31}$$

where a and θ are parameters giving the maximum slope of

$$max[S'(x)] = S'(\theta) = \frac{a}{4} \tag{32}$$

This is the subpopulation response function chosen for the analysis in [5], if any other sigmoid function was taken the details of solutions would be different.

To calculate the slope, an assumption can be made that the slope of equation (29) at S_ϵ^{-1} be greater than zero. The slope of the isocline at this point is then

$$\frac{c_1}{c_2} - \frac{9}{a_\epsilon c_2} \tag{33}$$

This leads to the condition $c_1 > \frac{9}{a_\epsilon}$ where a_ϵ is slope parameter for the excitatory response function.

The following theorem as seen in [5] can be stated: if $c_1 > \frac{9}{a_\epsilon}$, then there is a class of stimulus configurations such that the isoclines as defined in equations (29) and (30) will have at least three intersections. This means that there are at minimum three steady state solutions in equations (27) and (28). A detailed proof can be found in [5].

In Figure 6, the two steady states are separated by an unstable one. The same parameters are used for Figure 7. Here the solid lines represent stable states while the dashed ones indicate instability. The arrows indicate the hysteresis loop.

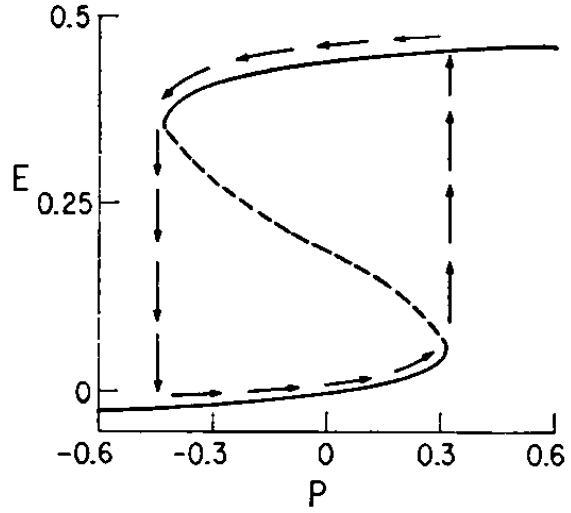

Figure 7: Steady state values for E as a function of P with $Q = 0$. Solid lines represent stable states and dashed lines represent unstable states. The arrows indicate the hysteresis loop. ([5] fig 5)

Changing the parameters to $c_1 = 13$, $c_2 = 4$, $c_3 = 22$, $c_4 = 2$, $a_\epsilon = 1.5$, $\theta_\epsilon = 2.5$, $a_i = 6$, $\theta_i = 4.3$, $r_\epsilon = r_i = 1$, and $P = Q = 0$ gives 5 steady states as seen in Figure 8. The condition for 5 steady states is

$$\frac{a_\epsilon c_2}{a_\epsilon c_1 - 9} > \frac{a_i c_4 + 9}{a_i c_3} \tag{34}$$

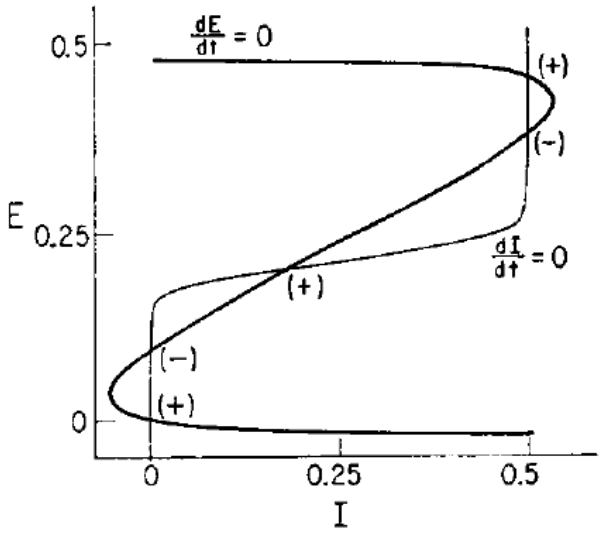

Figure 8: Nullclines where parameters meet the condition for 5 steady states ([5] fig 8)

3 Modelling with Gaussian Activation Function

In [3], Meijer et al model epileptic activity using a model based on the Wilson-Cowan model. In this case a Gaussian function is used instead of sigmoid.

3.1 Study Observations

In this study the participants were observed during seizure activity. Micro-electrodes were surgically implanted into the participants heads (the participants in this study had tried other treatment methods). Plots of the recordings show that the activation function is a mix of a sigmoid function and a Gaussian function with a maximum. The firing rate index (FRI) which is the average electrical activity is plotted in Figure 9 against the signal from the electrode called the low frequency component.

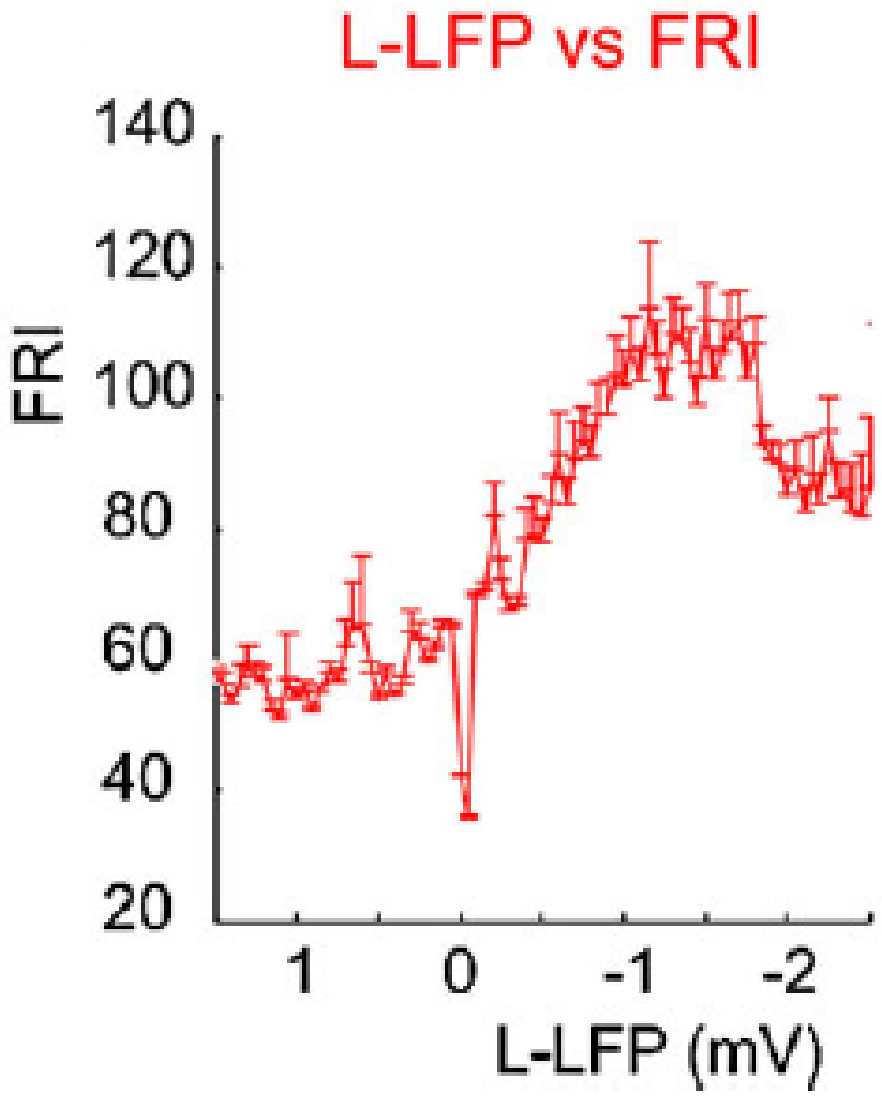

Figure 9: Plot of firing rate index (FRI) vs low frequency component (L-LFP) ([3] fig 1C)

An assumption that the number of spikes is not dependent on the input current is made for simplification. Given that the input current has a finite range, a Gaussian function is obtained when summing over an entire population.

3.2 Local Microcircuit Modelling

The local microcircuit model with both excitatory and inhibitory neurons is given by the following,

$$\tau_E E_k' = -E_k + (1 - E_k)F_E(J_{E_k}) \tag{35}$$

$$J_{E_k} = w_{EE}E_k - w_{IE}I_k + \beta + \alpha w_{EE}(E_{k+1} + E_{k-1}) \tag{36}$$

$$\tau_I I_k' = -I_k + (1 - I_k)F_I(J_{I_k}) \tag{37}$$

$$J_{I_k} = w_{EI}E_k - w_{II}I_k \tag{38}$$

where $k = 1, 2, ..., N$. The currents are give by J_{E_k} and J_{I_k}.E_θ and I_θ denote the threshold levels, and E_{sd}, I_{sd} the standard deviations. The values of the parameters will be the same as seen in previous studies [3]. Taking $\tau_E = \tau_I = 1, w_{EE} = 16, w_{EI} = 18, w_{II} = 3, w_{IE} = 12, E_\theta = 7, I_\theta = 5, E_{sd} = 2.1$ and $I_{sd} = 1.5$. The Gaussian functions are given by

$$F_E(J_{E_k}) = exp\left(-\left(\frac{J_{E_k} - E_\theta}{E_{sd}}\right)^2\right) - exp\left(-\left(\frac{-E_\theta}{E_{sd}}\right)^2\right) \tag{39}$$

$$F_I(J_{I_k}) = exp\left(-\left(\frac{J_{I_k} - I_\theta}{I_{sd}}\right)^2\right) - exp\left(-\left(\frac{-I_\theta}{I_{sd}}\right)^2\right) \tag{40}$$

and the sigmoid functions by

$$F_E(J_{E_k}) = (1 + exp(-E_s(J_{Ek} - E_\theta)))^{-1} - (1 + exp(E_s E_\theta))^{-1} \tag{41}$$

$$F_I(J_{I_k}) = (1 + exp(-I_s(J_{Ik} - I_\theta)))^{-1} - (1 + exp(I_s I_\theta))^{-1} \tag{42}$$

The values of the parameters for the sigmoid functions are $E_\theta = 5.2516$, $E_s = 1.5828$, $I_\theta = 3.7512$ and $I_s = 2.22$.

3.2.1 Spatially continuous model

Replacing $E_k(t)$ and $I_k(t)$ by $E(y,t)$ and $I(y,t)$ respectively, then the input currents are given by the following functions,

$$J_E(y,t) = \lambda_E \int_0^L \left[w_{EE}e^{|y-z|/\sigma_{EE}}E(z,t) - w_{IE}e^{|y-z|/\sigma_{IE}}I(z,t)\right] dz + B(y,t) \tag{43}$$

$$J_I(y,t) = \lambda_I \int_0^L \left[w_{EI}e^{|y-z|/\sigma_{EI}}E(z,t) - w_{II}e^{|y-z|/\sigma_{II}}I(z,t)\right] dz \tag{44}$$

where $y \in [0, 1000\mu m]$ and $w_{EE} = 2, w_{IE} = 1.65, w_{EI} = 1.5, w_{II} = 0.01, \sigma_{EE} = 70\mu m, \sigma_{IE} = 90\mu m, \sigma_{IE} = 90\mu m, \sigma_{II} = 70\mu m, E_\theta = 18, E_{sd} = 6.7, I_\theta = 10$ and $I_{sd} = 3.2$.

To compare to the sigmoid function, $E_\theta = 12.41, E_{sd} = 2, I_theta = 7.33, I_{sd} = 0.95$ and density is $\lambda_E = \lambda_I = 1\mu m^{-1}$.

3.3 Analysis

3.3.1 One E-I pair

The phase plane analysis for the equations in section 3.2 with $\beta = 3$ are given in Figure 10. The excitatory nullcline is similar for both the Gaussian and sigmoid activation functions in terms of shape. For the inhibitory nullcline, the sigmoid activation function has monotonic shape while the Gaussian one has a hump.

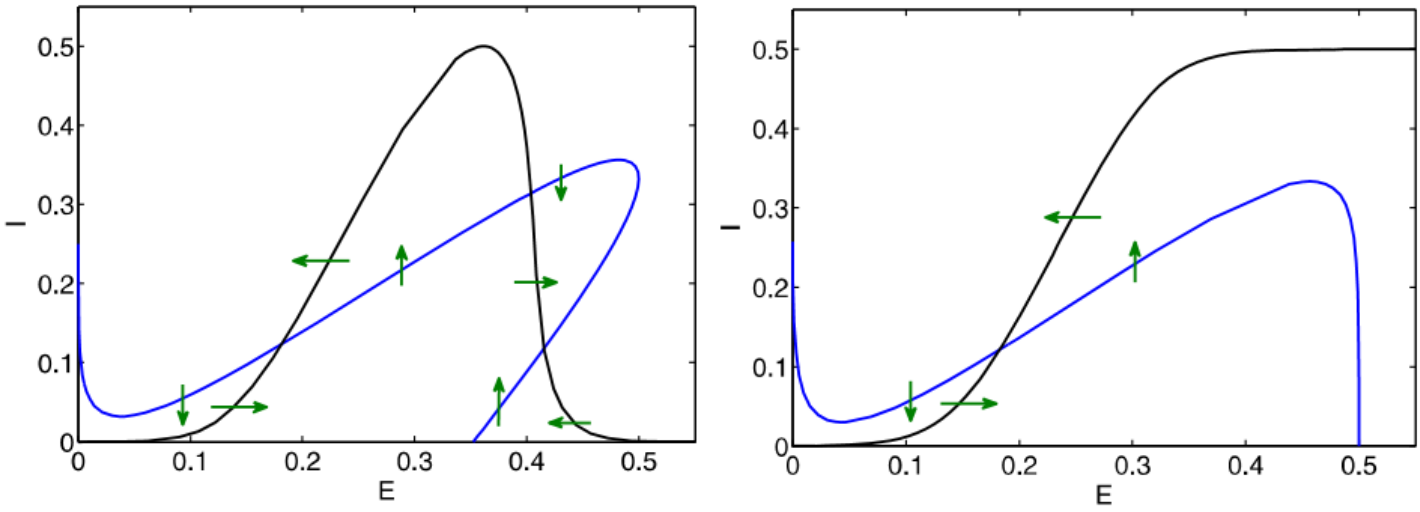

Figure 10: Phase plane analysis for Gaussian (left) and sigmoid (right). The E-nullcline is in blue and the I-nullcline is in black. ([3] fig 4)

There is one critical point at around $(0.2, 0.15)$ for both the Gaussian and sigmoid activation functions. The Gaussian activation function has two more points, a saddle at around $(0.4, 0.3)$ and a stable node at $(0.41, 0.1)$. This stable node is something that exists with usual Wilson-Cowan dynamics with a sigmoid function. Bifurcation diagrams varying w_{EI} and β can help to show this. The bifurcation diagrams are similar to ones done on a sigmoid function in a previous study. The Gaussian diagram (see Figure 11) shows a saddle-node bifurcation curve corresponding to the steady state. This occurs with high values of w_{EI} and lower values of β. The excitatory population drives the inhibitory population to the depolarization block.

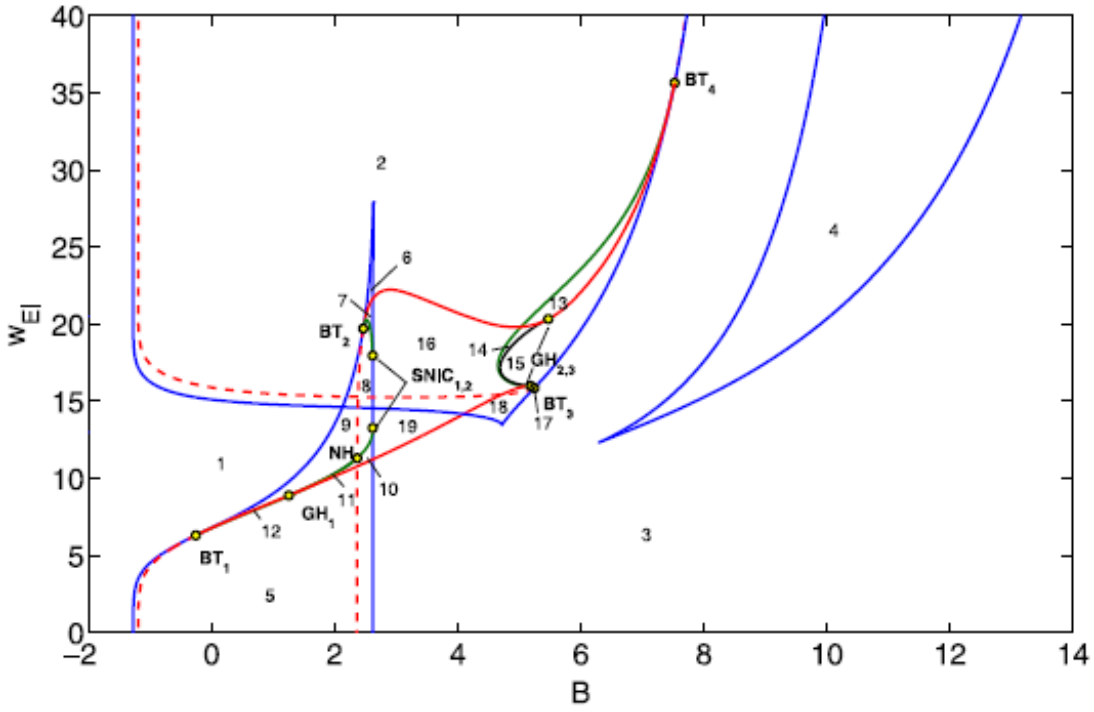

Figure 11: Bifurcation diagram for Gaussian function. The colours indicate the bifurcations curves. Saddle-node (blue), Hopf (red), limit points of the cycles (black), homoclinic to saddle (green) and neutral saddle (dashed red line). ([3] fig 5)

3.3.2 Two E-I pairs

The bifurcation diagrams for two excitatory coupled E-I pairs are done by fixing $w_{EI} = 18$ so that an additional steady state happens and by varying α and β. α is the coupling strength between excitatory populations so negative values are not neurophysiologically relevant but can be shown. When $\beta = 2.45$, there are two equilibrium states, one with high excitatory activity and the other with low. For $\beta = 3$, there is the high equilibria and a stable oscillation state.

Looking at Figure 12, at around $\alpha = 0$ and $E \approx 0.01$ there is a solid black steady state line. This occurs until $\alpha \approx 0.33$ where there is an unstable saddle-node, denoted SN_1. Another stable area is between the pitchfork bifurcations, PF_1 at $\alpha \approx -0.647$ and PF_2 at $\alpha \approx 1.13$. Then unstable from PF_2 until the stable saddle-node SN_3 at $\alpha \approx 0.86$. PF_1 to SN_2 at $\alpha \approx 0.502$ is also unstable. Then the supercritical Hopf bifurcation, H at $\alpha \approx 0.255$. Lastly, there is a stable asymmetric in-phase oscillation branch that ends in a saddle-node.

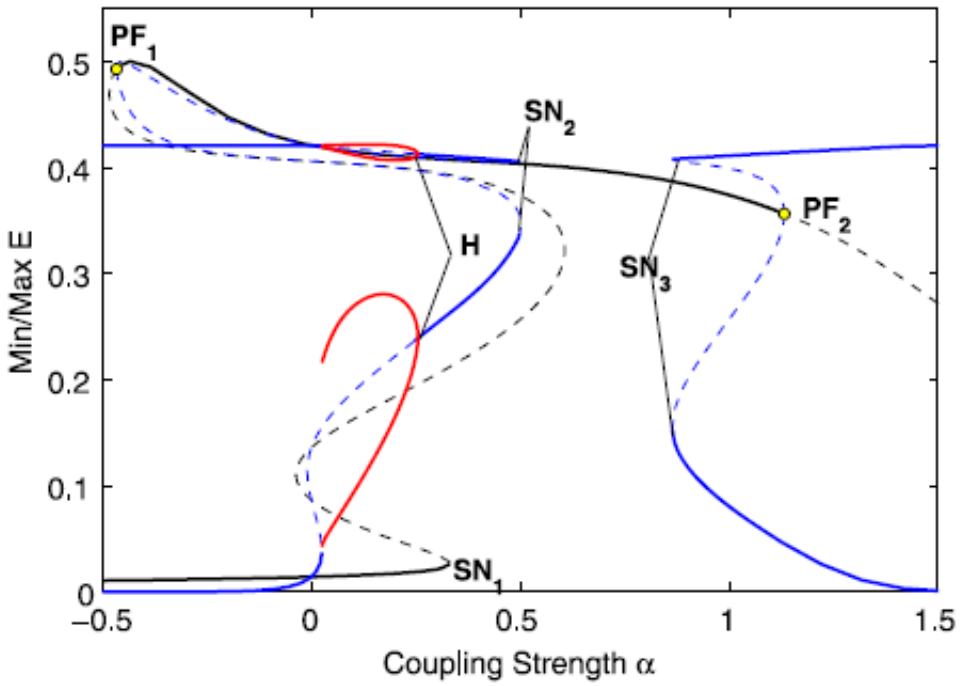

Figure 12: Bifurcation diagram for $\beta = 2.45$. The colours indicate the solution type. Symmetric (black) and asymmetric (blue) steady states and in-phase asymmetric oscillations (red). The dashed lines indicate unstable branches. ([3] fig 7)

When $\beta = 3$, the steady states are similar. Between PF_1 and PF_2 there is a high symmetric steady state but the lower one is unstable. There is also a similar in-phase asymmetric oscillation at H_1.

3.3.3 Spatially continuous model

The analysis of a model with 2 populations shows that stable asymmetric in-phase oscillations occurs. The simulation can also be repeated for a larger network with 25 populations. Setting $\beta = 2.3$ and $\alpha = 0.1$ and putting all the populations in a steady low activity equilibrium. E_{12} receives additional stimuli by adjusting β_{12} and this population switches to a steady state with high activity. This forces the neighbouring populations into an oscillatory mode analogous the the asymmetric in-phase oscillation. Since the remaining cell populations remain in low activity the oscillation is localized.

β is increased to 2.45 and the simulation is repeated. As the cycles occur 3 or more populations enter oscillatory mode. The waves end when the boundary is reached or several populations

are active simultaneously. When $\beta = 3$, the oscillation is not local, instead the entire network is driven by one population.

In Figure 13, the simulations from the spatially continuous model are shown. The top row is the sigmoid firing response function. The middle is the Gaussian activation function and the bottom is also Gaussian at different times.

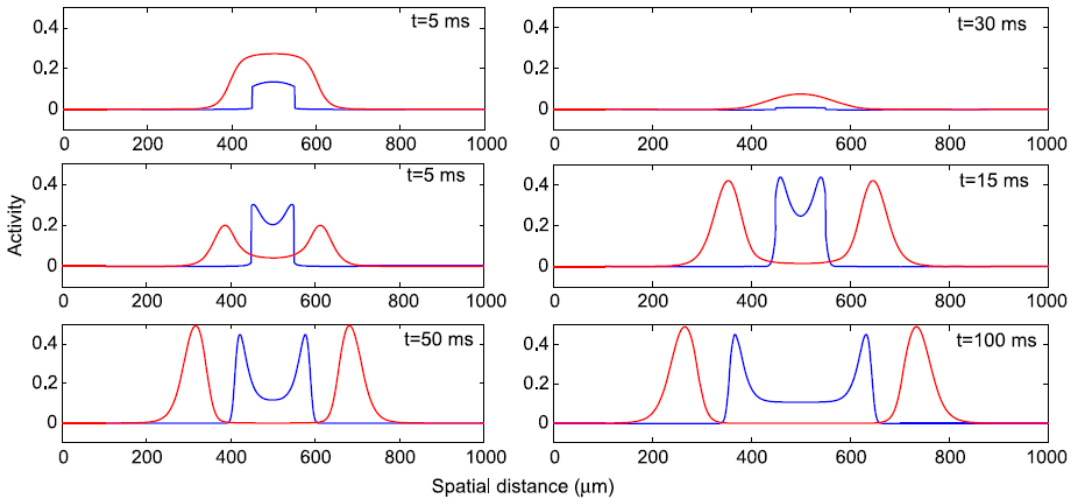

Figure 13: Spatially continuous model diagrams ([3] fig 11)

In conclusion, for equilibrium, which activation function is chosen is not important. What matters is that the inhibitory firing rate function has a maximum and drops off. But of course, this is just one way to model. There are also other computational models.

4 Simulations and Mean Field Model

In [7], models are used to simulate the activity of neurons. A mean field model is then derived to verify the simulations.

4.1 Simulation

Two models were used to stimulate neurons. One was the Morris-Lecar(M-L) and the other was Hodgkin-Huxley(H-H) [7]. The H-H neuron models the system through the opening and closing of voltage-gated ion channels, while the M-L neuron replaces the channels with voltage dependent functions. Modification of M-L neuron parameters means the excitatory neurons are regularly spiking while the inhibitory neurons are fast spiking and the inhibitory neurons

are more susceptible to the depolarization block than the excitatory ones[7]. The modified M-L model used in the simulation replaces the calcium ion channel with a sodium ion (Na^+) channel.

The M-L model can be represented by a system of differential equations with the membrane potential V and the potassium activation channel w,

$$C\frac{dV_i}{dt} = -g_{N_a}m(V_i)(V_i - E_{N_a}) - g_k w(t)(V_i - E_k) - g_{Cl}(V_i - E_{Cl}) + I_i^{ext}(t) + I_i^{syn}(t) \quad (45)$$

$$\frac{dw}{dt} = \phi\frac{w_\infty(V_j) - w}{\tau_\infty} \quad (46)$$

where $m(V) = (1+\tanh((V-V_1)/V_2))/2, w_\infty(V) = (1+\tanh((V-V_3)/V_4))/2, \tau_\infty = 1/\cosh((V-V_5/(2V_6)))$. The values for all the parameters can be found in a table in [7]. As seen in Figure 14 there are 3 main states dependent on I_{ext},

i. rest state (in solid black) when I_{ext} is low

ii. limit cycle (in red)

iii. depolarization block (solid black) when I_{ext} is high

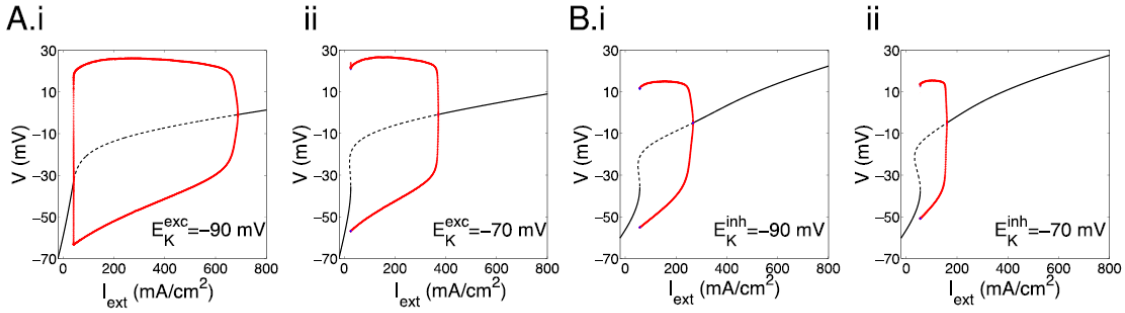

Figure 14: Bifurcation diagrams for Morris-Lecar neuron model. For the excitatory neurons in A.i. $E_k = -90mv$ and in A.ii. $E_k = -70mv$. Similarly for the inhibitory neurons in B.i. $E_k = -90mv$ and in B.ii. $E_k = -70mv$. The solid and dashed black lines indicate stable and unstable fixed points. The red lines indicate the max and min of limit cycles. ([7] fig 1)

4.2 Mean Field Model

The mean firing rates are given by

$$\frac{dr_e}{dt} = -r_e + \phi_e\left(J_{ee}r_e - J_{ei}r_i + I_{ext}^E\right) \quad (47)$$

$$\tau\frac{dr_i}{dt} = -r_i + \phi_i\left(J_{ie}r_e - J_{ii}r_i + I_{ext}^I\right) \quad (48)$$

with the following activations functions

$$\phi_e(x) = \frac{1}{1+e^{-x}} \tag{49}$$

$$\phi_i(x) = \frac{1}{1+e^{-x}} \frac{1}{1+e^{k(x-\theta)}} \tag{50}$$

The coupling strengths are given by J_{ee}, J_{ei}, J_{ie} and J_{ii} from one population to another and τ is the time constant. The external inputs are given by I^E_{ext} and I^I_{ext}. In Figure 15, the excitatory activation function is a sigmoid function (in black). As the depolarization block threshold decreases so does the maximum value of the function. θ is reduced from 10 (blue), then 8 (green) and then 6 (red). In the mean field model, the parameter θ is akin to E_k in the M-L model.

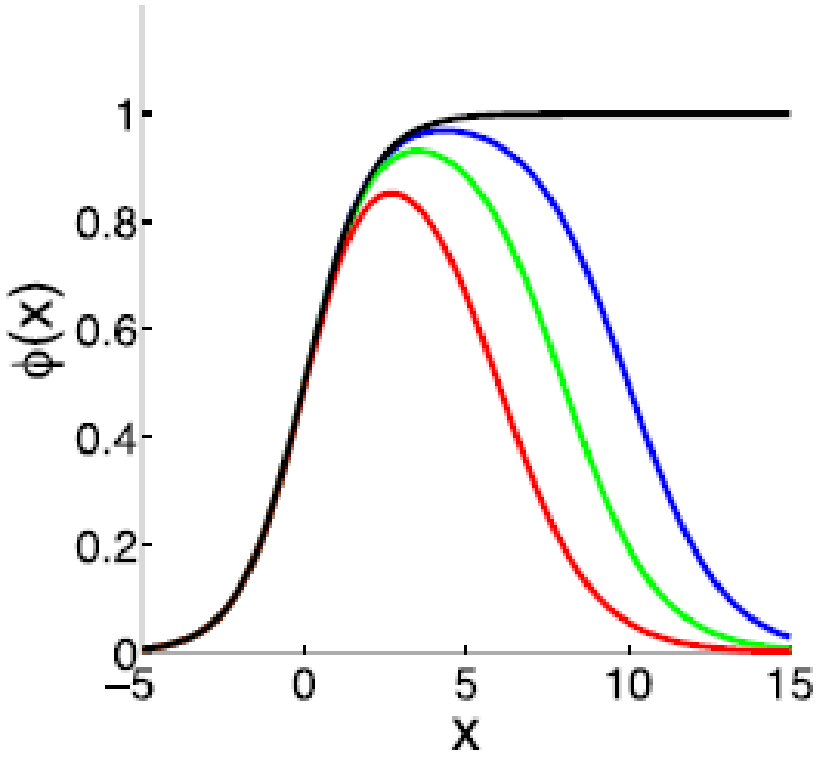

Figure 15: Activation function for mean field model for different values of θ ([7] fig 2)

The phase plane diagram for the mean field model can be seen in Figure 16A with two stable fixed points. The normal state b_1 and the seizure state b_2. The seizure state occurs when there is excessive excitatory activity while the inhibitory population is in the depolarization block.

At the point b_2, r_e is at its maximum and r_i is near zero. The removal of the seizure state can be seen in Figure 16B and in Figure 16C. In B, the external input is reduced, so $I^E_{ext} = -7$ and there is one stable fixed point. In C, $\theta = 10$.

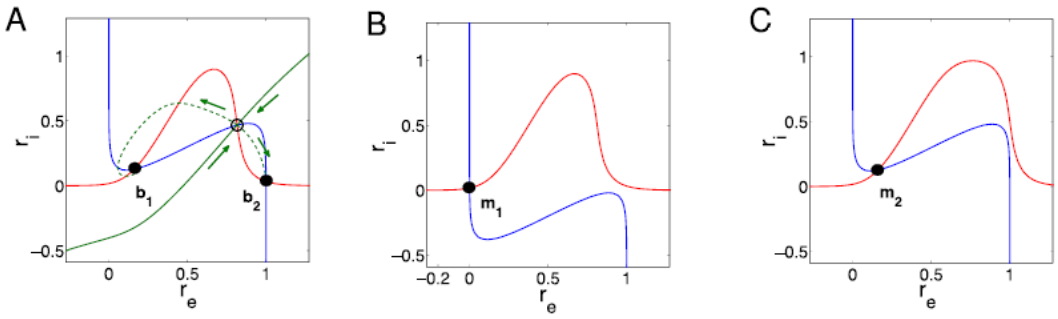

Figure 16: Phase plane diagrams for the mean field model. The r_e-nullcline is in blue and the r_i-nullcline is in red. ([7] fig 3)

The mean field model helps to analyse the transitions between seizure states and other non-seizure states. The bifurcation diagram for a low value of θ can be seen in Figure 17A.i. If the external input, I^I_{ext} is sufficiently large, then the transition to seizure is made via a saddle-node bifurcation as shown in the phase plane diagram in Figure 17A.iii. The middle figure shows a bifurcation diagram for a higher value of θ. When exiting the seizure state, the inhibitory firing rate makes a strong rebound and the excitatory firing rate drops from maximum to normal.

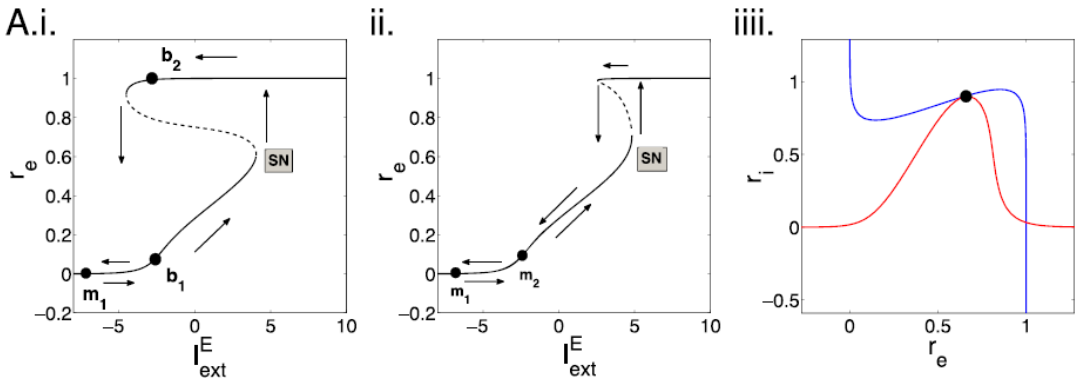

Figure 17: Bifurcation diagrams and phase plane ([7] fig 4)

This demonstrates that before a seizure, inhibition is strong.

5 Conclusion

For the field of computational neuroscience, the Wilson-Cowan equations are an important landmark [8]. More than 50 years later they are still begin used, for example by Meijer et al in [3] and by Chow and Karimipanah in [8].

5.1 Wilson-Cowan Model

The Wilson-Cowan equations model the local population dynamics of neurons. What sets this model apart from previous ones is the interactions between the two subpopulations [5]. However this model still has limitations including the neglect of spatial interactions seen in a later paper [8] and the assumption that the relative refractory period is 0.

5.2 Gaussian Activation Function Model

The model in [3] shows the the activation function is mix of sigmoid function and a Gaussian function. The microcircuit model used to examine the two activation functions shows that the excitatory population drives the inhibitory population the the depolarization block. After expanding the microcircuit model to include multiple populations, the conclusion that the type of activation function does not matter. Whatever function is chosen, needs an inhibitory firing rate function with a maximum that drops off.

One limitation of this model is that it does not describe the transition between certain states.

5.3 Neuron Simulation and Mean Field Model

In [7], the H-H and M-L neurons models were used to stimulate neurons. The mean field model was used to verify the simulation. The M-L neurons show that to reach the depolarization block, the external input for the inhibitory neurons is lower. The mean field models show the conditions for the existence of both a seizure and normal state. Removal of the seizure state is also shown along with transition to a seizure state via a saddle-node bifurcation.

One limitation of the M-L neurons simulation, is the dynamics of potassium were not modelled. For the mean field model, mapping between single cell dynamics and population dynamics is lacking.

5.4 What Comes Next

Looking at Figure 10 and Figure 16, the phase plane diagrams, it can be observed that the excitatory nullcline (blue in both figures) has similar curves. The curves in Figure 16 are more similar to the sigmoid curve in Figure 10. Recall that in Figure 10, the inhibitory nullcline is in black and in Figure 16 it's in red. The inhibitory nullcline from Figure 16 is more similar to the Gaussian activation function's curve in Figure 10. It would be interesting to see the model in neuron simulation and field model with a Gaussian activation function in order to compare to the sigmoid one. However in both [3] and [7], stable and seizure states can coexist. Strong inhibition also comes before an epileptic wave.

The modelling of seizure activity is important as epilepsy affects about 1% of the population [3] and currently mechanisms behind seizures are not known. Better understanding could lead to potential improvements for those for whom current treatment it is unsuccessful.

References

[1] Molnar C and Gair J.2015. Concepts of Biology[Internet]. 1st Canadian Edition. BCcampus[cited 2021 May 31] Available from https://opentextbc.ca/biology/

[2] Weitan W, McCann D.Psychology: Themes and Variations. 4th Canadian. Nelson Education Ltd; 2016

[3] Meijer HGE, Eissa TL, Kiewiet B et al. Modeling Focal Epileptic Activity in the Wilson–Cowan Model with Depolarization Block. Journal of Mathematical Neuroscience. 2015 [accessed 2020 Nov 1];Vol.5(7) doi:10.1186/s13408-015-0019-4

[4] Moustafa A. 2018. Computational Models of Brain and Behaviour[Internet]. John Wiley & Sons[cited 2021 May 31]. Available from https://ebookcentral-proquest-com.proxy.library.carleton.ca/lib/oculcarleton-ebooks/detail.action?pq-origsite=primo&docID=5046842

[5] Wilson HR, Cowan JD. Excitatory and Inhibitory Interactions in Localized Populations of Model Neurons. Biophysical. 1972 [accessed 2020 Nov 1];Vol.12(1):p1-24. doi: 10.1016/S0006-3495(72)86068-5

[6] Witelski T, Bowen M. 1015. Methods of Mathematical Modelling[Internet]. Springer [cited 2020 Sept 9]

[7] Kim CM, Nykamp DQ. The influence of depolarization block on seizure-like activity in networks of excitatory and inhibitory neurons. Journal of Computational Neuroscience.2017 [accessed 2021 March 17] Vol.43(1), 65-79. doi: 10.1007/s10827-017-0647-7

[8] Chow CC, Karimipanah Y. Before and beyond the Wilson–Cowan equations. Journal of neurophysiology. 2020 [accessed 2020 Nov 1];Vol.123(5):p1645-1656. doi: 10.1152/jn.00404.2019

[9] Sayama H. Introduction to the Modeling and Analysis of Complex Systems. Available from https://math.libretexts.org/Bookshelves/Scientific_Computing_Simulations_and_Modeling/Book%3A_Int